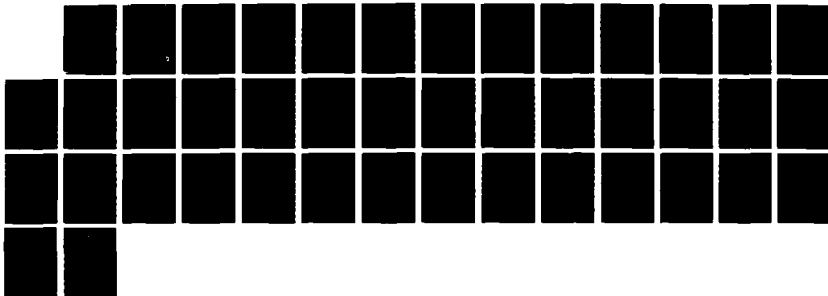AD-A190 870   EFFECTS OF TOROIDAL FORCES IN CURRENT LOOPS EMBEDDED IN   1/1
              A BACKGROUND PLASMA(U) NAVAL RESEARCH LAB WASHINGTON DC
              J CHEN 29 DEC 87 NRL-MR-6086
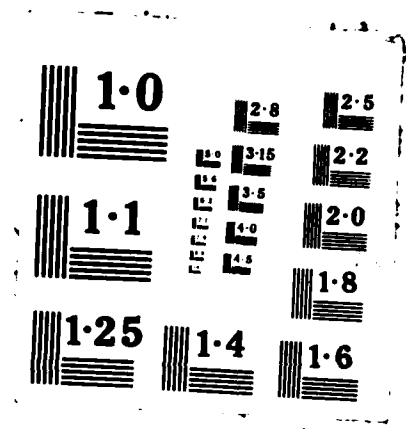
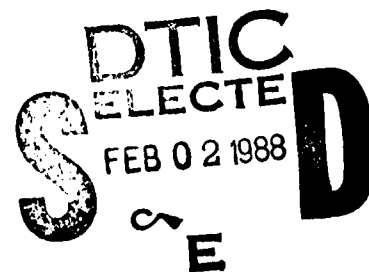UNCLASSIFIED   F/G 20/9   NL

AD-A188 878

Effects of Toroidal Forces in Current Loops Embedded in a Background Plasma

JAMES CHEN

Geophysical and Plasma Dynamics Branch
Plasma Physics Division

December 29, 1987

DTIC
SELECTED
FEB 0 2 1988
E

88 1 27 037

REPORT DOCUMENTATION PAGE

1a REPORT SECURITY CLASSIFICATION	1b RESTRICTIVE MARKINGS
UNCLASSIFIED	

2a SECURITY CLASSIFICATION AUTHORITY	3 DISTRIBUTION AVAILABILITY OF REPORT
2b DECLASSIFICATION DOWNGRADING SCHEDULE	Approved for public release; distribution unlimited.

4 PERFORMING ORGANIZATION REPORT NUMBER(S)	5 MONITORING ORGANIZATION REPORT NUMBER(S)
NRL Memorandum Report 6086	

6a NAME OF PERFORMING ORGANIZATION	6b OFFICE SYMBOL (If applicable)	7a NAME OF MONITORING ORGANIZATION
Naval Research Laboratory	Code 4780	

6c ADDRESS (City, State, and ZIP Code)	7b ADDRESS (City, State, and ZIP Code)
Washington, DC 20375-5000	

8a NAME OF FUNDING/SPONSORING ORGANIZATION	8b OFFICE SYMBOL (If applicable)	9 PROCUREMENT INSTRUMENT IDENTIFICATION NUMBER
Office of Naval Research		47-0884-07

8c ADDRESS (City, State, and ZIP Code)	10 SOURCE OF FUNDING NUMBERS			
	PROGRAM ELEMENT NO	PROJECT NO	TASK NO	WORK UNIT ACCESSION NO
800 No. Quincy Street Arlington, VA 22203	61153N	RR033-02-44		DN880-024

11 TITLE (Include Security Classification)

Effects of Toroidal Forces in Current Loops Embedded in a Background Plasma

12 PERSONAL AUTHOR(S)
Chen, James

13a TYPE OF REPORT	13b TIME COVERED		14 DATE OF REPORT (Year, Month, Day)	15 PAGE COUNT
Interim	FROM ___	TO ___	1987 December 29	42

16 SUPPLEMENTARY NOTATION

17	COSATI CODES		18 SUBJECT TERMS (Continue on reverse if necessary and identify by block number)
FIELD	GROUP	SUB GROUP	Three-dimensional semi-toroidal current loop
			High-temperature stratified background plasma
			Loop structures

19 ABSTRACT (Continue on reverse if necessary and identify by block number)

> A study is made of dynamical properties of a three-dimensional semi-toroidal current loop embedded in a high-temperature stratified background plasma. The model loop carries a toroidal current density J_t and poloidal current density J_p, producing the magnetic field components B_p and B_t, respectively. Starting with a non-forces-free current loop in stable MHD equilibrium described by $c^{-1} J \times B - \nabla p = 0$ where the major radial forces as well as the minor radial forces are explicitly balanced, the dynamical properties resulting from major radial perturbations are investigated. The analysis is first carried out using a class of three-dimensional semi-toroidal equilibria previously identified. It is found that some equilibrium loops are unstable to such perturbations, resulting in major radial expansion. The condition for instability is given in terms of a "circuit" parameter ϵ which is a measure of the flux associated with the overall current distribution. The resulting motion is due to the toroidal geometry of the current loop and is determined by the Lorentz force, pressure gradient and drag force due to the ambient gas. For the equilibrium loops studied, the motion is found to be subsonic. Time evolution of the loops and the magnetic energy converted via drag heating are presented.

(Continues)

20 DISTRIBUTION AVAILABILITY OF ABSTRACT	21 ABSTRACT SECURITY CLASSIFICATION
☒ UNCLASSIFIED/UNLIMITED ☐ SAME AS RPT ☐ DTIC USERS	UNCLASSIFIED

22a NAME OF RESPONSIBLE INDIVIDUAL	22b TELEPHONE (Include Area Code)	22c OFFICE SYMBOL
J. D. Huba	(202) 767-3630	Code 4780

DD Form 1473, JUN 86   Previous editions are obsolete   SECURITY CLASSIFICATION OF THIS PAGE

S/N 0102-LF-014-6603

i

19. ABSTRACT (Continued)

Results are also presented for loops with relatively strong current and magnetic fields which are not in equilibrium initially. It is found that for sufficiently large current, a current loop can be driven supersonically through the background gas, accompanied by shocks and rapid shock heating of the ambient gas. The wide range of dynamical behavior exhibited by current loops, and the pros and cons of the model are discussed in the context of current loops in the solar corona.

CONTENTS

Accession For

NTIS GRA&I	X
DTIC TAB	☐
Unannounced	☐
Justification	

By

Distribution/

Availability Codes

| Dist | Avail and/or Special |
| A-1 | |

QUALITY
INSPECTED
2

EFFECTS OF TOROIDAL FORCES IN CURRENT LOOPS EMBEDDED IN A BACKGROUND PLASMA

I. INTRODUCTION

Observation shows that the solar corona is filled with complicated structures. It is generally believed that magnetic fields and currents play important roles in the structuring and dynamics of the coronal plasmas. Among the wide variety of possible configurations, loop-like structures have received considerable attention because of their prevalence and relative simplicity. In addition, the Skylab (1973) results indicate that a significant number of flare events may be associated with bipolar magnetic structures. Loop structures have also been studied in the context of coronal heating and loop-type coronal transients. Some of the possible loop structures include simple loops, loops embedded in complex structures and arcades of loops. In addition, it has been suggested that magnetic loops may play a role in the structure of other astrophysical objects such as the coronae of accretion disks (Galeev, Rosner, and Vaiana 1979). It is clear that properties of loop-like magnetic and current structures can have profound implications for the dynamics of plasmas in the solar corona and similar astrophysical systems.

Much work has been done to investigate the properties of various loop-like structures such as their MHD, thermal and radiative properties. This paper will primarily deal with certain MHD aspects. In the area of MHD studies, a considerable of amount of work has been done on equilibrium loop models as can be found in a number of reviews including Priest(1981), Brown and Smith(1980), Sturrock(1980) and Svestka(1976), and numerous references contained therein. Although magnetic structures are generally complex, simplified geometries have been used to study the basic properties. One configuration that has received considerable attention is that of discrete current loops (e.g., Chiuderi, Giachetti, and Van Hoven, 1977; Hood and

Priest 1979). In these works, bipolar loops were approximated by straight cylinders. However, it is known (Krall and Trivelpiece 1973) that current-carrying plasmas with curvature experience certain forces which arise from the slight imbalance in the $\underline{J}x\underline{B}$ and $\underline{\nabla}p$ forces, henceforth referred to as "toroidal forces". Thus, by using straight-cylinder approximations, these forces due to curvature were neglected. Other tractable models often studied include force-free configurations (see, for example, Sakurai 1981; Aly 1984; Yang, Sturrock, and Antiochos 1986). However, more realistic systems are generally three-dimensional and need not be force-free. As a result, attempts have been made to generalize to three-dimensional non-force-free configurations. For example, Low (1985a; 1985b) discussed a class of three-dimensional structures. In addition, Low (1982) discussed an isolated current loop embedded in a field-free plasma. However, in these models, the current in the solar radial direction is zero so that these models are restrictive.

An important property of a solar current loop is that it has curvature, giving rise to toroidal forces. This aspect of MHD forces has received only limited attention. Previously, Xue and Chen (1983), henceforth refered to as Paper 1, considered the MHD equilibrium and stability properties of current loops embedded in a background plasma. In this work, one class of non-force-free "semi-toroidal" equilibria which satisfies $c^{-1}\underline{J} \times \underline{B} - \underline{\nabla}p = 0$ was studied. The intrinsic curved geometry and the toroidal forces were explicitly taken into account. It was found that toroidal equilibrium force balance imposes geometrical constraints on physical quantities such as pressure and magnetic field. Figure 1 shows a schematic drawing of an isolated current loop. The subscripts "t" and "p" refer, respectively, to the toroidal and poloidal components of $\underline{J}$ and $\underline{B}$. One interesting property of this class of equilibria is that they are stable to gross MHD modes. Specifically, it was found that the stability conditions for the sausage mode, kink mode and the Mercier criterion are satisfied. This is consistent with the apparent longevity of some loop-like structures in the solar corona. For some other MHD stability considerations, see, for example, Priest (1979) and Van Hoven (1981).

Loop models have also been developed for phenomena exhibiting a wide range of motion such as coronal transients (MacQueen et al., 1974). Mouschovias and Poland (1977) proposed a model of freely moving loops with

2

the magnetic forces balanced by gravity. Anzer (1978) and Van Tend (1979) used a simple ring current driven by the Lorentz force. This force is similar in nature to the toroidal forces discussed in Paper 1. In Anzer's model, an idealized current loop carrying only a toroidal current was used, without poloidal current and pressure gradient. By considering the resulting Lorentz force and gravity, the dynamics of the apex of the loop were studied. It was found that a weak magnetic field of the order of 1G is sufficient to drive coronal transients to velocities of several hundred kilometers per second. No MHD equilibrium consideration of the initial

loop was given in this work. Yeh and Dryer (1981) noted that a net force in the major radial direction is insufficient to drive a loop unless the force acts to accelerate each element of the loop plasma. They then proposed that buoyant force may play an important role. However, a current distribution with curvature can undergo net traslational motion in the major radial direction under the action of the toroidal forces referred to earlier (see, for example, Krall and Trivelpiece 1973) with the pressure gradient providing the coupling of the plasma elements.

In point of fact, numerous energetic effects showing varying degrees of motion do occur in the solar corona. For example, slow loop expansion may take place prior to flares, followed by rapid expansion at flare onset. In addition, mass motion may be manifested in the form of Type II and Type IV bursts, coronal mass ejections, etc. For less dramatic effects, quasi-stationary magnetic loops may exhibit much slower motion. The significance and possible mechanisms of "mechanical energy" output in the flare energy budget have been discussed extensively in a review paper by Webb et al (1980) and references contained therein. Because the corona is essentially fully ionized, we expect that mass motions and magnetic fields are integrally related.

Toroidal forces are not new. They occur in any curved segments of current-carrying plasmas. In the laboratory, these forces are well-understood. However, laboratory plasmas are typically surrounded by vacuum which in turn is enclosed in rigid metallic containers. In addition, magnetic fields are applied by external coils to balance the toroidal forces. In the solar and astrophysical environments, magnetic and current structures are usually embedded in plasmas, and are not surrounded by metallic containers. The effects of toroidal forces in such environments

3

have not been fully investigated. The question which is the motivation of this paper is how the toroidal forces may act in solar current loops, and if and under what conditions these forces may be important.

In Paper 1, some equilibrium aspects of the toroidal forces were considered. In the present paper, we will study the dynamical behavior of a model current loop. In order to elucidate the physics of toroidal forces unambiguously, we will construct the simplest possible model that can isolate the essential effects of toroidal forces. The model consists of a

current loop embedded in a field-free background plasma. How does such a current loop behave under the action of toroidal forces alone ? That is the scope and the question we address in this paper. As a result, we will neglect from the present calculation some properties which are not directly related to the toroidal froces. For example, the possible interaction of the current loop with the ambient magnetic fields (see, for example, Mouschovias and Poland, 1977; Osherovich and Gliner 1983) will not be considered. The role of gravity will not be emphasized because toroidal forces occur with or without gravity and, for the examples in this paper, it turns out to be unimportant. However, gravity can be included for the dynamics of the apex in a straightforward manner and will be discussed briefly (Sec. IV). The understanding gained here can then serve as a basis for generalizing the model to more complex and realistic systems.

We will start with a current loop which is initially in equilibrium and calculate its time-dependent behavior in response to perturbations of the major radius (Sec. II). The theoretical framework will be first presented, followed by a numerical calculation of the long-time evolution of loops including the drag force due to the ambient gas (Sec. III). We then discuss the behavior of a loop carrying a relatively large current, which may not be in equilibrium initially. Although no attempt to model specific systems will be made, we will discuss the potential relevance of the results to plasma activities in the corona (Sec. IV). It will be shown that a current loop acting under the influence of toroidal forces can mimic certain dynamical effects in which plasma motion is important.

II. DYNAMICS OF A MODEL CURRENT LOOP

In the present analysis, we consider the evolution of an isolated
current loop which is initially in stable MHD equilibrium. The equilibrium
and stability properties of one class of current loops have been discussed
in Paper 1. Figure 1 shows schematically a model current loop with a
toroidal current density J_t and poloidal current density J_p. The
associated magnetic field components are B_p and B_t, respectively. The loop
is embedded in a high-temperature plasma of pressure p_a. We allow the
current to close in or below the photosphere to satisfy current
conservation. Thus, the current loop is such that its lower part is
anchored in a much denser plasma. However, no particular current
distribution will be specified below the photosphere.

The ambient plasma is assumed to have a gravitational scale height
H. In the solar corona, H is given by

$$H = \frac{2kT_a}{m_i g} ,$$

where k is the Boltzman constant, T_a is the ambient plasma temperature, m_i
is the ion mass and g is the gravitational acceleration which is 2.7×10^4 cm
$\sec^{-2}$ at the surface. At the base of the corona, H is of the order of 10^5
km.

A. Toroidal Forces

As discussed in Paper 1, a semi-torus of a uniform radius of curvature
(major radius) R and a minor radius a is used to model the basic toroidal
properties of a current loop. We assume that the aspect ratio is large
with R/a of 5 to 10. The local force density $\underline{f}$ acting on an element of the
loop is given by

$$\underline{f} = \frac{1}{c} \underline{J} \times \underline{B} - \underline{\nabla}p, \tag{1}$$

where $\underline{J} = (c/4\pi)\underline{\nabla} \times \underline{B}$. In this paper, the displacement current is
neglected. We integrate $\underline{f}$ over a section of the torus to obtain the major
radial force per unit length (Shafranov, 1966):

5

$$F = -\frac{I_t^2}{c^2 R} \left[\ln \left(\frac{8R}{a}\right) + \beta_p - \frac{3}{2} + \frac{\ell_i}{2} \right], \qquad (2)$$

where F acts in the major radial direction and I_t is the total toroidal current defined by

$$I_t = 2\pi \int_0^a dr \, r J_t.$$

The quantity β_p is defined by

$$\beta_p = \frac{\bar{p} - p_a}{B_p^2/8\pi}, \qquad (3)$$

where $\bar{p}$ is the average internal pressure of the loop, p_a is the ambient pressure and $B_p = B_p(a)$ is the poloidal magnetic field at the outer edge of the loop (r = a). Note that the toroidal effects are relatively insensitive to the assumption of uniform R/a because of the logarithmic dependence. The quantity ℓ_i is the internal inductance term, characterizing the minor radial current distribution, and ℓ_i ranges from 0 for a surface distribution to 1/2 for a uniform current distribution. In eq. (2), mass flow along the loop is also neglected because the toroidal forces occur with or without such flow. Moreover, mass flow is important only if the flow velocity is comparable to the Alfven speed in the loop. The above expressions (also eqs. [31] and [32] to be used later) are appropriate for current-carrying plasmas embedded in a conducting plasma with no metallic containers and properly satisfy the requirements of the virial theorem (Shafranov, 1966). As noted before, this is an important difference from such laboratory systems as tokamaks. These equations do not depend on the detailed minor radial distribution of current and pressure. Only averaged or integrated quantities such $\bar{p}$ and ℓ_i are needed.

As the initial configuration, we will adopt a model equilibrium loop of the type discussed in Paper 1. In this class of equilibrium loops, the toroidal forces are explicitly balanced. Here, we give a brief summary of equilibrium and stability properties. In equilibrium, the force density $\underline{f}$ acting on each element of the loop is zero. Therefore, we have F = 0 in equation (2). This then gives

$$\beta_p = -\ln \left(\frac{8R}{a}\right) + \frac{3}{2} - \frac{\ell_i}{2}. \qquad (4)$$

6

Since $\ell_i/2$ is smaller than the other terms, we will adopt, for convenience, a surface current model and set $\ell_i = 0$ henceforth. For R/a of the order of 10, we see that $\beta_p < 0$ in equilibrium. It is convenient to define the total poloidal current by

$$I_p = 2\pi R \int_0^a dr\ J_p.$$

For the surface current model, we have

$$B_t = \frac{2I_p}{cR} \tag{5}$$

with $B_p = 0$ and $p = \bar{p}$ inside the loop. Outside the loop, we have

$$B_p = \frac{2I_t}{cr} \tag{6}$$

with $B_t = 0$ and $p = p_a$. Using these expressions, β_p can be calculated from equation (3). It is also easy to see that, in equilibrium,

$$\beta_p = 1 - B_t^2(0)/B_p^2(a). \tag{7}$$

This condition is determined from the minor radial equilibrium and has already been incorporated into equation (2). In the above expressions, the correction terms of the order a/R due to the simplification of half-torus above the photosphere are neglected. It can be shown that the stability conditions for the sausage mode, kink mode and the Mercier criterion are satisfied. For a more detailed discussion of equation (2) and the equilibrium/stability properties as applied to the solar environment, the reader is referred to Paper 1.

B. Dynamical Instability

In this section, we investigate the stability properties of the equilibrium loop with respect to major radial perturbations. In our simple model, the perturbation δR is applied uniformly to the semi-torus. In

7

reality, the footpoints are essentially immobile on the relevant time scales so that distortions in the semi-toroidal geometry will in the nonlinear stage. However, the toroidal effects are relatively insensitive to such distortions since they depend on the aspect ratio as $\ln(8R/a)$. In addition, for the analysis in this section, perturbation amplitudes can be arbitrarily small so that we expect the geometrical simplification to provide a good approximation to the linear behavior of the loop.

As the major radius is displaced from its initial equilibrium position, the forces experienced by the loop can be given by linearizing equation (2):

$$\frac{d^2(\delta R)}{dt^2} = \frac{I_t^2}{c^2 MR} \left(\frac{\delta R}{R} - \frac{\delta a}{a} + \delta\beta_p \right). \tag{8}$$

Here $M = \pi a^2 \bar{\rho}$, δa is the change in the minor radius and $\bar{\rho}$ is the average mass density inside the loop. The quantity $\delta\beta_p$ is obtained from equation (3):

$$\delta\beta_p = \frac{\delta\bar{p} - \delta p_a}{B_p^2/8\pi} - 2\beta_p \frac{\delta B_p}{B_p} , \tag{9}$$

where $\delta\bar{p}$ is the change in the average internal pressure and

$$\delta p_a = - \frac{\delta R}{H} p_a, \tag{10}$$

where H is the gravitational scale height.

Due to the small resistive dissipation, flux conservation is approximately satisfied. The toroidal flux conservation gives

$$B_t a^2 = \text{constant} \tag{11}$$

and the poloidal flux conservation gives

$$L_T I_t = \Phi_T = \text{constant}. \tag{12}$$

Here, Φ_T is the total poloidal flux and L_T is the total self-inductance of the current distribution including the submerged part (Figure 1). Note

that current conservation requires only that there be some current. Given a current, the total flux Φ_T and inductance L_T can be unambiguously defined (albeit not necessarily measured) without specifying details of the underlying current structure. We can define the inductance L_p associated with the poloidal flux above the photosphere by

$$L_p = \frac{\Phi_p}{I_t}$$

where the total poloidal flux is $\Phi_T = \Phi_p + \Phi_s$. Then, we define

$$\epsilon = \frac{\Phi_p}{\Phi_T} = \frac{L_p}{L_T}. \tag{13}$$

This quantity ϵ is a rough measure of the relative "size" of the loop above the phot phere and the entire current structure. Note that the inductance L_s of the submerged current is not calculated. It is used as a parameter to characterize the gross circuit effects.

We have described the essential ingredients of the model. We will now attempt to calculate more specific properties. In order to keep the physics transparent, we will assume minor radial equilibrium. This is not necessary for the analysis and, as will be seen later (Sec. III), gives an accurate result. For the dynamics of the loop interior, we assume that the current loop is thermally well-insulated from the corona on the relevant time scale so that the adiabatic expansion law is valid:

$$\bar{p} \, \bar{V}^\gamma = \text{constant}$$

where γ is the adiabatic index and where $\bar{V} = \pi^2 a^2 R$ is the volume of the loop. Then, we have

$$\delta \bar{p} = - \gamma \bar{p} \left(2 \frac{\delta a}{a} + \frac{\delta R}{R} \right). \tag{14}$$

Next, from toroidal flux conservation, equation (11), we obtain

$$\frac{\delta B_t}{B_t} = - 2 \frac{\delta a}{a}. \tag{15}$$

From the definition of B_p, we find

9

$$\frac{\delta B_p}{B_p} = \frac{\delta I_t}{I_t} - \frac{\delta_a}{a} \, . \tag{16}$$

It is convenient to note that $\delta\beta_p$ can be rewritten as

$$\delta\beta_p = 2(1 - \beta_p)\left[- \epsilon(1 - \hat{L}^{-1}) + (1 + \epsilon\hat{L}^{-1})(\tfrac{R}{a}\tfrac{da}{dr})\right] \frac{\delta R}{R} \, ,$$

where $\hat{L} = \ln(8R/a) - 2$. In order to find δI_t, we assume that the changes in the total inductance are primarily due to changes in the loop above the photosphere since the submerged current structure is much less mobile, being embedded in a much denser plasma. Then, we have

$$\delta L_T \simeq \delta L_p .$$

From equation (12), we obtain

$$\frac{\delta I_t}{I_t} = - \epsilon \frac{\delta L_p}{L_p} \, , \tag{17}$$

where $\epsilon = L_p/L_T$. For a semi-toroidal plasma of major radius R and minor radius a ($r/a \gg 1$), we have (Bateman, 1978)

$$L_p = \frac{2\pi R}{c^2} \left[\ln\left(\tfrac{8R}{a}\right) - 2\right] \tag{18}$$

with $\ell_i = 0$ and

$$\frac{\delta I_t}{I_t} = - \epsilon \left\{1 + \hat{L}^{-1}\left[1 - \tfrac{R}{a}(\tfrac{da}{dR})\right]\right\} \frac{\delta R}{R} \, ,$$

In order to determine da/dR, we must relate the changes in the pressure to changes in the field. Using the expression for β_p and variations in the pressure terms, we obtain

$$\delta\bar{p} - \delta p_a = 2(1 - \beta_p) \frac{B_p^2}{8\pi} \left(\frac{\delta B_p}{B_p} - \frac{\delta B_t}{B_t}\right) + 2\beta_p\left(\frac{B_p^2}{8\pi}\right) \frac{\delta B_p}{B_p} \, .$$

Combining the preceding results and after some straightforward algebra, we find

$$\frac{da}{dR} = \frac{a}{2R} \left[\epsilon \frac{B_p^2}{8\pi} \hat{L}^{-1} + (1 - 2\beta_p) \frac{B_p^2}{8\pi} + \gamma\bar{p} \right]^{-1} \left[2\epsilon(1 + \hat{L}^{-1}) \frac{B_p^2}{8\pi} + \frac{R}{H} p_a - \gamma\bar{p} \right].$$

(19)

For the parameter values to be used later, this quantity is roughly 0.1 even when the expansion velocity is not infinitesimal. Using these results in equation (8), we finally obtain the linearized equation for major radial perturbation:

$$\frac{d^2(\delta R)}{dt^2} = \frac{I_t^2}{c^2 MR} \left\{ 1 - \left(\frac{R}{a} \frac{da}{dR}\right) + 2(1 - \beta_p)\left[(1 + \epsilon\hat{L}^{-1})\left(\frac{R}{a} \frac{da}{dR}\right)\right.\right.$$

$$\left.\left. - \epsilon(1 + \hat{L}^{-1})\right] \right\} \frac{\delta R}{R} .$$

(20)

If we set $\epsilon = 0$ in this equation, we find that the right hand side is positive, indicating that the perturbation can grow. If we set $\epsilon = 1$, we find that $(R/a)(da/dR) \ll 1$ for typical value for solar current loops (e.g., $R \sim 10^5$ km, $a \sim 10^4$ km, $p_a \sim$ a few dynes cm^{-2}). Thus, the right hand side of equation (20) is negative. This means that the loop is stable to major radial perturbations. Thus, there exists a quantity ϵ_{cr} with

$$0 < \epsilon_{cr} < 1$$

(21)

such that the $d^2(\delta R)/dt^2 = 0$ for $\epsilon = \epsilon_{cr}$. By setting the right hand side of equation (20) equal to zero and after some algebra, we find

$$\epsilon_{cr} = - \left[(1 - 2\beta_p)\left(\frac{R}{H} p_a - \gamma\bar{p}\right) + 2\left(\frac{B_p^2}{8\pi}\right)(1 - 2\beta_p) + 2\gamma\bar{p} \right]$$

$$\times \left\{ - 2\left(\frac{B_p^2}{8\pi}\right) + 2(1 - \beta_p)p_a\hat{L}^{-1}\left[\frac{R}{H} - 2\gamma \ln\left(\frac{8R}{a}\right) + \gamma\right]\right.$$

$$\left. + 4\left(\frac{B_p^2}{8\pi}\right)(1 - \beta_p)\hat{L}^{-1}\left[\frac{1}{3} \beta_p \ln\left(\frac{8R}{a}\right) - (\gamma - \frac{1}{2})\beta_p\right] \right\}^{-1}.$$

(22)

A current loop with $\epsilon < \epsilon_{cr}$ is unstable to major radial perturbations and a loop with $\epsilon > \epsilon_{cr}$ is stable. For solar current loop parameters, ϵ_{cr} is typically 0.1 to 0.2 (Sec. III). The quantities ϵ and ϵ_{cr} are important for the dynamics of current loops and have the following simple physical

interpretation. For $\epsilon < \epsilon_{cr} \ll 1$, the loop above the photosphere is a small fraction of the entire current distribution. As the loop expands, the changes in the loop magnetic field and average internal pressure are relatively small in comparison with the changes in the ambient pressure. In particular, $\delta\beta_p > 0$ so that the loop is unstable. For $\epsilon > \epsilon_{cr}$, the loop is a larger fraction of the total current. The magnetic field and internal pressure decrease more rapidly in such a way that the displacement is restored. In a sense, this is simply a statement that the behavior of the loop depends on the rest of the "circuit". The essential ingredient for this effect is that the current structure is embedded in two distinct regions, one dense and the other much less dense.

For the unstable case, equation (20) yields the exponential growth time τ given by

$$\tau = \left(\frac{c^2 MR}{I_t^2}\right)^{1/2} \left\{ 1 - \left(\frac{R}{a}\frac{da}{dR}\right) + 2\left(1 - \beta_p\right)\left[\left(1 + \epsilon\hat{L}^{-1}\right)\left(\frac{R}{a}\frac{da}{dR}\right) \right. \right.$$
$$\left. \left. - \epsilon\left(1 + \hat{L}^{-1}\right)\right]\right\}^{-1/2}. \tag{23}$$

It is significant to note that $\tau \propto I_t^{-1}$ so that unstable loops with larger I_t linearly grows faster. Note also that MR is the total mass in the semi-toroidal loop so that it is independent of time since we assume no mass flow to or from the submerged regions. For the stable case, the loop can oscillate about the equilibrium position.

At this point, it is useful to consider the energy budget of a dynamically evolving current loop. The total magnetic energy of the semi-toroidal loop above the photosphere is the sum of the poloidal magnetic energy E_p and toroidal magnetic energy E_t where

$$E_p = \frac{1}{2} L_p I_t^2, \tag{24}$$

and

$$E_t = \frac{B_t^2}{8\pi}\left(\pi^2 a^2 R\right), \tag{25}$$

with L_p given by equation (18). Using the principle of virtual work, we find

$$F_p = \frac{\pi I_t^2}{c^2} \left[\ln\left(\frac{8R}{a}\right) - 1 \right], \tag{26}$$

and

$$F_t = \frac{\pi I_t^2}{2c^2} \left(\beta_p - 1 \right), \tag{27}$$

where F_p and F_t are the major radial forces acting on the entire loop due to $J_t B_p$ and $J_p B_t$, respectively. It is straightforward to show that the total pressure force in the major radial direction is

$$F_{\underline{\nabla}p} = \frac{\pi I_t^2}{2c^2} \beta_p. \tag{28}$$

Figure 2 shows the various local force components. Locally, the two components of the Lorentz force are both along the minor radius as shown. However, when these forces are integrated over the toroidal volume, we see that $J_t B_p$ contribution points outward along the major radius (eq. [26]) and $J_p B_t$ contribution points inward (eq. [27]). This is entirely due to the curvature of the current distribution. If we add these three forces and divide it by πR to get the total force per unit, then we recover equation (2), providing a heuristic derivation. The expression for F_p shows that as the major radius expands, the B_p component does work on the loop, losing energy to the loop. At the same time, the loop does work on the B_t component so that the B_t component gains energy as the loop expands. Because the minor radius expands, the internal gas and B_t do work against the ambient pressure and lose energy. On balance, there is a net loss of poloidal magnetic energy to the kinetic energy of the loop. A fraction of this energy is then converted to thermal energy via drag heating.

C. The Behavior of an Expanding Current Loop

In the preceding section, we have described the major radial stability properties of a model current loop embedded in a gravitationally stratified background plasma. In this section, we will discuss a simple picture of the long-time behavior. The scaling behavior obtained here will be useful for interpreting the numerical results to be discussed in the next section.

13

As the loop expands, the velocity of the apex increases and the drag on the ambient gas becomes important. As a simple model, we write (Tritton, 1977)

$$F_d = c_d(n_a m_i a V^2),$$ (29)

where F_d is the drag force per unit length, $V = dR/dt$ is the velocity of the loop (i.e., the apex), n_a is the local ambient density and c_d is the drag coefficient. An order-of-magnitude estimate for the characteristic velocity in the nonlinear expansion phase can be obtained by equating F_d to the driving force F given by equation (2). We note that the quantity in the square brackets is of order unity and we obtain

$$V_* \sim I_t (c_d m_i c^2 n_a a R)^{-1/2}.$$ (30)

After a period of expansion, a loop may attain saturation velocities of the order of V_*. Some loops may not saturate nonlinearly. Some loops may reach "second" stable equilibrium after periods of expansion.

Equation (30) shows that V_* is proportional to $I_t/n_a^{1/2}$. If we estimate V_* by taking $I_t = 5 \times 10^{10}$ A, $n_a = 4 \times 10^9$ cm^{-3}, R $= 10^5$ km, a $= 10^4$ km and using $c_d = 1$, then we find $V_* \sim 2 \times 10^2$ km sec^{-1}. It is of interest to compare this value, an order-of-magnitude estimate, to the sound speed C_s in the corona:

$$C_s = (\gamma \frac{2kT_a}{m_i})^{1/2}.$$

For $T_a \sim 2 \times 10^6$ K and $\gamma = 5/3$, $C_s \sim 2.4 \times 10^2$ km sec^{-1}. Although the actual expansion velocity depends on ϵ, the above comparison indicates that the peak velocity of the apex can be of the order of the sound speed under the action of toroidal forces. It will turn out that equilibrium loops of the type used here can only produce subsonic expansion. However, if a loop is allowed to be out of equilibrium initially, carrying a sufficiently large I_t, then it can be driven supersonically, or super-Alfvenically for magnetized ambient plasmas.

14

III. EVOLUTION OF MODEL CURRENT LOOPS

In the preceding sections, we have discussed in detail the linear dynamics of toroidal current loops in a background plasma. The analysis is limited to the linear behavior ($\delta R/R \ll 1$) and the description of the long-time behavior has been confined to scaling laws. We will now attempt to provide a more quantitative discussion of the nonlinear behavior by numerically integrating the equations of motion for the model loop. Numerical examples compatible with the solar environment are given to illustrate the range of behavior under the action of toroidal forces. The basic physics, however, is not limited to the sun.

As an initially semi-toroidal loop expands, the anchoring of footpoints in the photosphere cause the loop to deviate from the semi-toroidal geometry. The aspect ratio is no longer uniform. However, inclusion of non-uniform expansion would complicate the analysis unnecessarily inasmuch as the basic toroidal forces are affected only as $\ln(8R/a)$ by geometrical distortions, a mild dependence on the aspect ratio. The correction due to geometry is expected to be quantitative, rather than qualitative. In our analysis, we do not consider the geometrical distortions. Accordingly, the applicability of the results will be limited to the dynamics of the apex, which remains nearly semi-toroidal. This limitation is similar to that of Anzer (1978). For an improved geometry, see, for example, Anzer and Poland (1979). Although we do not calculate the motion of the loop near the footpoints, the inductance relates the dynamics of the apex and the rest of the current.

In the analysis of Sec. II, we have used the minor radial equilibrium condition, equation (7). As the expansion velocity increases, however, the so-called ram-pressure contribution becomes important. To allow the possibility of rapid expansion, we calculate the dynamics of the minor radius separately. We replace equation (2) with (Shafranov 1966)

$$\frac{d^2 a}{dt^2} = \frac{I_t^2}{\pi c^2 a^3 \bar{n} m_i} \left(\frac{B_t^2}{B_p^2} - 1 + \beta_p \right) \tag{31}$$

15

$$\frac{d^2R}{dt^2} = \frac{I_t^2}{\pi c^2 a^2 R \bar{n} m_i} [\ln(\frac{8R}{a}) + \frac{1}{2}\beta_p - \frac{1}{2}\frac{B_t^2}{B_p^2} - 1] - c_d(\frac{2an_a m_i}{\pi M})v^2, \quad (32)$$

where β_p, B_t and B_p are defined by equations (3), (5) and (6),
respectively. Because we assume that there is no net mass flow into the
loop, we have taken the quantity πMR, the total mass of the loop above the
photosphere, as constant in time. Higher order nonlinearities are
neglected for simplicity. In equilibrium, we recover equations (2) and
(4). We have directly integrated the above set of equations for a variety
of loop parameters. We have found that equation (7) is nearly true even
for velocity V up to $0.5C_s$. As indicated by equation (19), da/dt is found
to be typically one tenth of dR/dt so that the minor radius is essentially
in equilibrium for small to moderate dR/dt. This justifies, a posteriori,
the use of minor radial equilibrium in the perturbation analysis.

The drag coefficient c_d is based on a simple model of a straight
cylinder transverse to the flow in a compressible gas. For the subsonic
regime with a Reynolds number R_e of 10^6 to 10^8, c_d is 0.5 to 1 (see, for
example, Tritton 1977). As the velocity approaches Mach 1, c_d rapidly
attains a maximum value of approximately 2 at Mach 1 and decreases rapidly
for larger Mach numbers (Hoerner 1951). Physically, the drag term in
equation (32) is the force which the magnetically maintained cylinder
experiences in displacing the ambient gas. The supersonic drag coefficient
is obtained from Hoerner (1951).

In our calculation, the ambient gas is field-free. For the case with
ambient magnetic fields, the drag coefficient c_d must be modified and, for
super-Alfvenic motion, MHD shocks are generated. We do not treat the
shocks per se here. The physical picture is simply that if the loop apex
is driven supersonic or super-Alfvenic, then shocks are generated. In
addition, we believe that this treatment is in fact a reasonable
approximation unless the ambient fields are comparable to or exceed the
loop fields (~20G for the supersonic examples).

In Figure 3(a), we show the expansion velocity of the apex for a loop
with the initial equilibrium values $R_0 = 10^5$km, $a_0 = 2 \times 10^4$km and $I_t = 4.5$
$\times 10^{10}$ A, corresponding to $B_p = 4.5$G and $B_t = 8.1$G. This is a case with
relatively weak magnetic fields. The ambient pressure is taken to be $p_a = 2$ dyn cm^{-2} (e.g., an active region coronal gas) at $T = 2 \times 10^6$K so that the

number density is $n = 4 \times 10^9 \text{cm}^{-3}$. For this loop, we have $\varepsilon_{cr} = 0.2$ (eq. [22]). The values of ε significantly smaller than ε_{cr} should give rise to instability. Curves 1 and 2 correspond to $\varepsilon = 0.01$ and $\varepsilon = 0.05$, respectively. The velocity is normalized to the sound speed $C_s = 2.4 \times 10^2 \text{km sec}^{-1}$. These curves describe two loops of apparently identical appearance above the photosphere with different overall current structures. For Curve 1, the flux enclosed by the entire current distribution is one hundred times what is above the photosphere and for Curve 2, the total flux is 20 times what is above. Because of the low current and weak magnetic field, these loops do not expand rapidly. Although not shown here, these loops continue to expand slowly even after one hour with the major radius reaching 1.5 to 2 times the initial values. The expansion is nearly exponential for the first 20 minutes. In Figure 3(b), the major radial behavior is shown for the loops. In general, with other parameters being equal, loops with smaller values of $\varepsilon < \varepsilon_{cr}$ expand more rapidly to larger values of R, and in cases where loops can attain "second" equilibrium, they do so earlier and at smaller values of R. Also, as a loop expands, the expansion tends to slow down. One reason is that the current and magnetic field decrease. Another reason is that $\varepsilon(t)$ increases, reducing the tendency for instability and sometimes reaching a second equilibrium.

In Figures 4(a) and (b), we show the behavior of a smaller loop with $R_0 = 10^4 \text{km}$, $a_0 = 2 \times 10^3 \text{km}$. The current is $I_t = 4.5 \times 10^9 \text{A}$ so that $B_p = 4.5\text{G}$ and $B_t = 8.1\text{G}$. The magnetic field is the same as the case described in Figure 3. For this case, we find $\varepsilon_{cr} = 0.1$. Curve 1, corresponding to $\varepsilon = 0.01$, shows that the velocity reaches a maximum value of roughly $0.45C_s$ with a rise time of 4 minutes and decreases slowly for some time. During this time, the Lorentz force is nearly balanced by ∇p and the drag force. For $\varepsilon = 0.05$ (Curve 2), the velocity attains a maximum and vanishes at $t = 14$ min. Subsequently, the apex executes damped oscillation about a new equilibrium position, $R = 3 \times 10^4 \text{km}$. The period is roughly 5 min.

In general, smaller loops have shorter e-folding times (eq. [32]). This is because of the reduced inertia. Loops with larger currents I_t also have shorter e-folding times because of the increased Lorentz force. In Figures 5(a) and (b), we show an example with larger currents. The loop is

17

not in equilibrium initially. The parameters used are $R_0 = 10^5$km, $a_0 = 2 \times 10^4$km and $I_t = 2.1 \times 10^{11}$A so that $B_p = 21$G and $B_t = 22$G. The size is the same as the example in Figure 3 but the current and magnetic field are stronger. Curve 1 corresponds to $\epsilon = 0.01$ and the loop attains Mach 4 in about two minutes. The major readius increases to about 2×10^5km during this time. At t = 14 min, the apex velocity is approximately $V/C_s \cong 5$ or $V \cong 1200$km sec^{-1} and the major radius has increased to $R = 10 \times 10^5$ km. Subsequently, the expansion velocity slowly decreases over tens of minutes as the loop expands. Curve 2 corresponds to $\epsilon = 0.1$ and the configuration is slower than that described by Curve 1. The apex attains Mach 3.5, the maximum velocity, in about 2 minutes. The velocity then slowly decreases from ~600 km s^{-1} to ~200 km s^{-1} in about 30 minutes as the loop expands. For smaller currents, the velocities are smaller. From Figures 3 ¬ 5, it is clear that a wide range of behavior is possible under the action of toroidal forces.

In the examples given in Figures 3 and 4, the major radius expansion has been relatively limited so that the errors due to geometrical distortions are expected to be minor. In Figure 5, the major radius increases to about 1×10^6 ¬ 2×10^6km. However, the sharpest increase in the velocity occurs for R less than about $2R_0$, with only moderate geometrical distortions. Therefore, we expect the essential behavior to be well described within the geometrical simplification.

IV. PHYSICAL IMPLICATIONS AND DISCUSSION

We have described the dynamics of the apex of a model current loop embedded in a stratified background plasma. The structure is such that the semi-toroidal section of the loop is in the upper tenuous plasma while the remainder of the current distribution is embedded in the much denser plasma. The dynamical properties obtained are most applicable to the apex of the semi-toroidal loop. We have constructed the model in such a way that the model loop behavior is primarily determined by the toroidal forces. In this section, we will attempt to understand the possible roles the toroidal forces may play in the behavior of solar current loops. Clearly, the tenuous plasma would correspond to the corona and the dense lower background would correspond to the subphotospheric gases.

18

Observationally, it is not always easy to determine the magnetic structure or its motion. However, a signature of motion can be manifested as heating of coronal gas and moving gaseous material. Here, we will examine some possible observational implications. For this purpose, it is instructive and useful to consider the rate at which the magnetic energy is converted to thermal energy via the drag force. We have calculated the quantity

$$\frac{dE}{dt} = F_d \left(\frac{dR}{dt}\right)$$

for the model loops described in the preceding section. Here, F_d is the drag force given by equation (29) and dE/dt is the rate at which the ambient gas undergoes drag heating due to the apex motion. In calculating this quantity, we have assumed that only one third of the semi-torus around the apex is effective in drag heating. As the above expression indicates, the heating rate is proportional to V^3. We have also computed the time-integrated total energy which the magnetic field loses by accelerating the loop plasma and drag heating. This quantity is essentially equal to the time-integral of dE/dt and the loop kinetic energy. As pointed out before, the minor radial expansion is found to be about 1/10 of the major radial expansion so that it is negligible for the energy budget in comparison with the major radial expansion.

In Figure 6(a), we have plotted the energy release rate due to drag for the loop described in Figure 3(a). For $\epsilon = 0.01$ (Curve 1), the energy output rate is roughly 5×10^{25} erg sec^{-1} at $t = 20$ min and increases to 3×10^{26} erg sec^{-1}. During this time, the major radius increases from $1.2R_0$ to $2R_0$. Before $t = 20$ min, the loop exhibits only slow motion and insignificant energy output. For $\epsilon = 0.05$ (Curve 2) the loop motion is less pronounced with the energy release rate in the range of 10^{25} erg sec^{-1} during $t = 20$ min to $t = 30$ min. Figure 6(b) shows the time-integrated energy converted from the magnetic field to thermal and kinetic energy. For $\epsilon = 0.01$ (Curve 1), the total amount of magnetic energy released is roughly 3×10^{29} erg while, for $\epsilon = 0.05$ (Curve 2), it is 1.5×10^{29} erg. For both cases, roughly one half of the energy is in the form of thermal energy. In Figure 7(a), we show the drag heating rate for the loop described in Figure 4. For this case, the apex region of rapid motion is

smaller and the region for drag heating is correspondingly smaller. Thus, dE/dt is also smaller than the preceding case. For Curve 1 ($\varepsilon = 0.01$), the maximum heating rate is roughly 2.3×10^{24} erg sec^{-1} and it slowly decreases with time. For Curve 2 ($\varepsilon = 0.05$), the loop reaches a second stable equilibrium and no significant energy release takes place subsequently. Figure 7(b) gives the time-integrated total magnetic energy release. In Figure 8, we give the energy output profile for the loop described in Figure 5. For this loop, the magnetic field components are roughly 20G and the apex can be driven supersonic with correspondingly greater magnetic energy release. However, this loop is not initially in equilibrium in the context of the present model. For Curve 1 ($\varepsilon = 0.01$), the maximum energy release rate is roughly 10^{29} erg sec^{-1} with a time-integrated total of 2×10^{32} erg in 30 minutes. Curve 2 ($\varepsilon = 0.1$), shows an energy output profile in which the peak heating occurs in a duration of 10 minutes with a long decay phase lasting for tens of minutes. The total energy released is roughly 2×10^{31} erg in 30 minutes. For these two curves, there is a possibility of strong shock heating.

It is of interest to estimate the temperature of the ambient gas which is heated by the supersonic motion of the apex. For strong shocks ($M \gtrsim 3$), the temperature T_* behind the shock front can be determined by (Landau and Lifshitz, 1959)

$$\frac{T_*}{T_a} = \frac{[2\gamma M^2 - (\gamma-1)][(\gamma-1)M^2 + 2]}{(\gamma+1)^2 M^2},$$

where M is the Mach number of the shock and T_a is the ambient temperature. Taking $M \sim 3$ (Fig. 5(a)) and $\gamma = 5/3$, we find $T_* = 3.7 T_a$. Using $T_a = 2 \times 10^6$K, we find $T_* = 7.4 \times 10^6$K. For larger values of M, the temperature is higher. Thus, in this particular example (Curve 2), the coronal gas in the vicinity of the apex could be heated to approximately 10^7K and the heated blob of gas would be seen to be travelling away from the surface at ~ 700 km sec^{-1} with a peak value of ~ 800 km sec^{-1}. This phase can last for tens of minutes with the velocity and heating diminishing with time. For Curve 1, the velocity is considerably higher (~ 1200 km s^{-1}) with greater heating rate and temperature. The behavior of the heated gas suggested by Curve 2 of Figures 5 and 8 is reminiscent of

20

moving Type IV bursts. Curve 1 indicates the possibility that a loop can be driven by the toroidal forces to high velocities for extended periods of time, with the apex velocity levelling off at and slowly decreasing from several hundred kilometers per second. These velocities are suggestive of the velocities of fast coronal mass ejections (MacQueen et al 1974; Gosling et al 1974; Gosling et al 1976; Hildner 1977). Note that we do not imply any identification of the bright leading edges of CME's with bow shocks.

Anzer (1978) has described a loop-type transient model. The underlying physics is similar to that of our model in that both models use the Lorentz force to drive current loops. In Anzer's work, it was found that magnetic fields of 1G can drive coronal transients. In our model, we estimate the necessary magnetic fields to be greater. Because of some obvious differences such as the neglect of gravity in our analysis, precise comparisons are not attempted. Nevertheless, we can qualitatively understand the differences. In Anzer's model, the poloidal current density J_p and pressure gradient are neglected. In the toroidal geometry, the force $J_p B_t$ acts to counter the expansion of the apex. Furthermore, the ambient pressure which also acts to oppose the expansion is neglected. The only retarding force is gravity. In our examples, with magnetic fields of 10 - 20G in the lower corona for the supersonic examples (Figs. 5 and 8), gravity is unimportant (see below). Thus, Anzer's model tends to require smaller magnetic fields than our model to drive current loops to a given velocity. In addition, the current loops used by Anzer are much larger, initially $0.5R_\odot$ to $1R_\odot$. In our model, the magnetic field is also weaker at comparable altitutes. Taking, for example, Curve 1 of Figure 5, we find that at T = 30 min, R = $3R_\odot$, the magnetic field is roughly 8G. For Curve 2 at T = 30 min, R = $1.3R_\odot$, the magnetic field is roughly 4G.

In our model, the inclusion of ambient coronal gas allows conversion of magnetic energy to thermal energy. For Curve 1 of Figure 5, the expansion velocity is several hundred kilometers per second for tens of minutes and possibly much longer. Although the loops described by Figures 5 and 8 expand to the extent that the geometrical assumptions in the model are not likely to be valid, they do suggest that the toroidal forces may play a contributing role in dynamical effects such as coronal mass ejections. We reiterate that the behavior described here is primarily due to the toroidal forces.

In the examples treated in this paper, the role of gravity has not been considered. For some phenomena (e.g., coronal mass ejections), gravity may be important. For the apex of a loop, gravity acts along the major radius so that it is straightforward to include the gravitational force F_G where

$$F_G = \pi a^2 m_i g(n_a - \bar{n}). \tag{33}$$

Here, F_G is the gravitational force per unit length acting on the apex and g is the gravitational acceleration. For the sake of generality, we have included both the ambient density n_a and the average internal density $\bar{n}$. If $\bar{n} > n_a$ (e.g., coronal transients), F_G is downward. If $\bar{n} < n_a$, then the structure is buoyant and F_G is upward. Inclusion of gravity will tend to reduce the expansion velocities if $\bar{n} > n_a$. On the other hand, the current can be increased to enhance the expansion speed. In fact, for magnetic fields of 10 ¬ 20G, the toroidal forces dominate the gravitational force. For example, for the supersonic loop depicted in Figure 5 with a density of $10^9 cm^{-3}$, the toroidal forces are of the order of $10^{10} dyn\ cm^{-1}$ while F_G is of the order of $10^8 dyn\ cm^{-1}$. Thus, the basic tenets of toroidal effects remain qualitatively valid with the addition of gravity. In this paper, the objective is not to model specific phenomena such as coronal mass ejections but to understand unambiguously the general physical effects of toroidal forces in the solar environment and to describe the range of behavior that may be exhibited by current loops. The reader interested in the effects of gravity may include equation (33) in equation (32).

In summary, we have described the behavior of simple semi-toroidal current loops under the action of toroidal forces. It has been shown that such loops are capable of exhibiting a wide range of dynamical behavior. Starting with MHD equilibria with the toroidal forces explicitly balanced, loops can expand with a wide range of subsonic velocities and a correspondingly wide range of magnetic energy output. Some loops can attain second equilibria. The typical time scales for motion and energy release are tens of minutes. Given loops initially in equilibrium, the subsequent motion seems to be subsonic with relatively slow heating of the coronal gas. This process may contribute to coronal heating. If we start with nonequilibrium loops carrying large currents, they can attain highly

22

supersonic (or super-Alfvenic in magnetized ambient plasmas) expansion velocities with rapid heating due to shock heating. This process may play a contributing role in certain energetic processes following onset of flares (loss of equilibrium ?) such as loop expansion, moving Type IV bursts, and mass ejections.

A novel but somewhat unconventional feature of the model is the explicit inclusion of submerged current distributions in the dynamics of the loop. As pointed out previously, the present model does not depend on any details of the submerged current distributions. The influence of the submerged current on the loop dynamics is contained in the quantity ϵ , the ratio of inductances, defined by equation (13). The physical reason for this behavior is discussed in Sec. II.B. Although not measurable in reality, this is an unambiguously definable and physically meaningful quantity. An implication is that two loops of identical appearance above the photosphere can behave differently depending on the underlying current structures (i.e., different ϵ).

In our model, the current loop above the photosphere is connected to the submerged structure via magnetic flux tubes going through the photosphere. The flux tubes serve as a conduit for electromagnetic and other processes. Thus, the properties of the loop above the photosphere can be influenced by the underlying current. This is a plasma analogue of a "battery and wire" system with the battery inside a metallic box and the load outside. In fact, the submerged currents can also serve as an additional reservoir of magnetic energy in some cases. In this paper, we have not addressed the issues concerning the details of possible transport mechanisms in plasmas. An adequate consideration of these issues requires some knowledge of subphotospheric currents and plasma properties. One possibility might be that the subphotospheric magnetic structure associated with a current loop would consist of complex flux tubes which confine high magnetic fields determined by hydromagnetic force-balance and flux conservation. We have left these issues for future research.

The present analysis has been based on one class of equilibrium and certain nonequilibrium current loops. Much work is needed to identify other types of configurations and quantitatively assess the effects of toroidal forces. We have presented a simple model to illustrate the basic

23

physics and possible effects of toroidal forces. Various improvements, some of which have already been mentioned, need to be made before it can be realistic. Nevertheless, it appears that current loops under the action of toroidal forces can mimic certain energetic effects exhibiting motion in the corona.

Acknowledgments

References

Aly, J. J. 1984, Ap.J., 283, 349.

Anzer, U. 1978, Solar Phys., 57, 111.

Anzer, U. and Poland, A.I. 1979, Solar Phys., 61, 95.

Bateman, G. 1978, MHD Instabilities, The MIT Press, Cambridge, MA.

Brown, J. C. and Smith, D. F. 1980, Rep. Prog. Phys., 43, 125.

Chiuderi, C., Giachetti, R., and Van Hoven, G. 1977, Solar Phys., 54, 107.

Galeev, A. A., Rosner, R., and Vaiana, G. S. 1979, Ap. J., 229, 318.

Gosling, J. T., Hildner, E., MacQueen, R. M., Munro, R. H., Poland, A. I., and Ross, C. L. 1974, J. Geophys. Res., 79, 4581.

Gosling, J. T., Hildner, E., MacQueen, R. M., Munro, R. H., Poland, A. I., and Ross, C. L. 1976, Solar Phys., 48, 389.

Hildner, E. 1977, L. D. de Feiter Memorial STIP Symposium, Tel Aviv.

Hoerner, S. F. 1951, Aerodynamic Drag, Otterbein Press, Dayton, Ohio, P. 223.

Hood, A. W. and Priest, E. R. 1979, Astron. Astrophys., 77, 233.

Krall, N. A. and Trivelpiece, A. W. 1973, Principles of Plasma Physics, McGraw-Hill, Inc., New York.

Landau, L. D. and Lifshitz, E. M. 1959, Fluid Mechanics, Pergamon Press Inc., New York, P. 331.

Low, B. C. 1982, Ap. J., 263, 952.

Low, B. C. 1985a, Ap. J., 293, 31.

Low, B. C. 1985b, Solar Phys., 100, 309.

MacQueen, R. M., Eddy, J. A., Gosling, J. T., Hildner, E., Munro, R. H., Newkirk, G. A.,Jr., Poland, A. I., and Ross, C. L. 1974, Ap. J., 187, L85.

Mouschovias, T. Ch., and Poland, A. I. 1978, Ap. J., 220, 675.

Osherovich, V. A. and Gliner, E. B. 1983, Solar Phys., 96, 179.

Priest, E. R. (ed.) 1981, Solar Flare Magnetohydrodynamics, Gordon and Breach, New York.

Sakurai, T. 1981, Solar Phys., 69, 343.

Shafranov, V. D. 1966, in Reviews of Plasma physics, Vol. 2, Consultants Bureau, New York, 103.

Sturrock, P. A. (ed.) 1980, Solar Flares, Colorado Assoc. Uniov. Press, Boulder, Colorado.

Svestka, Z. 1976, Solar Flares, D. Reidel Publ. Co., Boston.

Tritton, D. J. 1977, Physical Fluid Dynamics, Van Nostrand Reinhold Co., New York, P. 29.

Van Hoven, G. 1981, in E. R. Priest (ed.), Solar Flare Magnetohydrodynamics, Gordon and Breach, New York.

Van Tend, W. 1979, Solar Phys., 61, 89.

Webb, D. F., Cheng, C.-C., Dulk, G. A., Edberg, S. J., Martin, S. F., McKenna-Lawlor, S., and McLean, D. J., 1980, in P.A. Sturrock (ed.), Solar Flares, Colorado Assoc. Univ. Press, Boulder, Colorado, P. 471.

Xue, M. L. and Chen, J. 1983, Solar Phys., 84, 119.

Yang, W. H., Sturrock, P. A., and Antiochos, S. K. 1986, Ap. J., 309, 383.
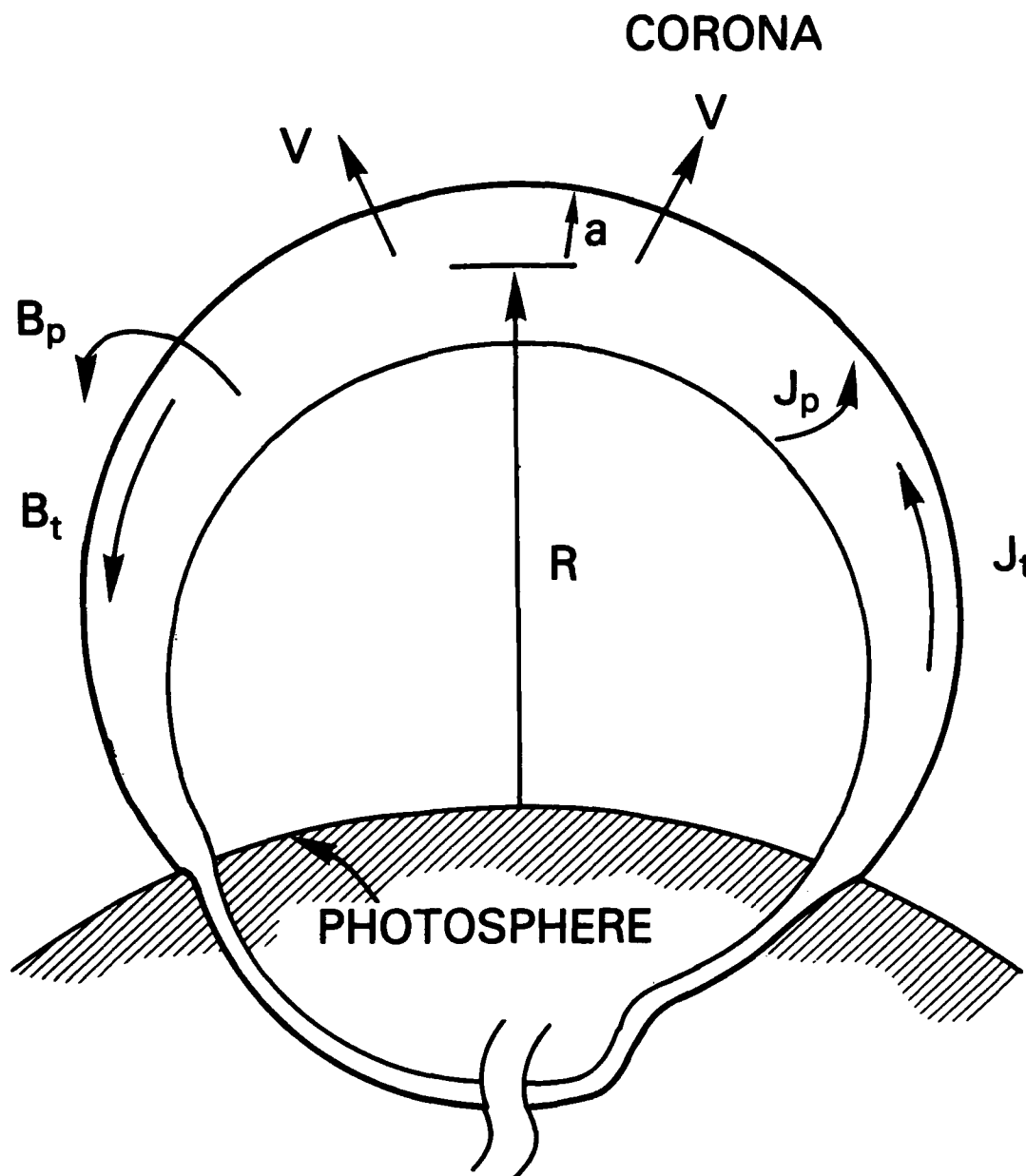
Yeh, T. and Dryer, M. 1981, Ap. J., 704.

Fig. 1   Schematic drawing of a model current loop embedded in the
          corona. Components of the current density $\underline{J}$ and magnetic
          field $\underline{B}$ are shown. The subscripts "t" and "p" refer to the
          toroidal and poloidal directions, respectively. No particular
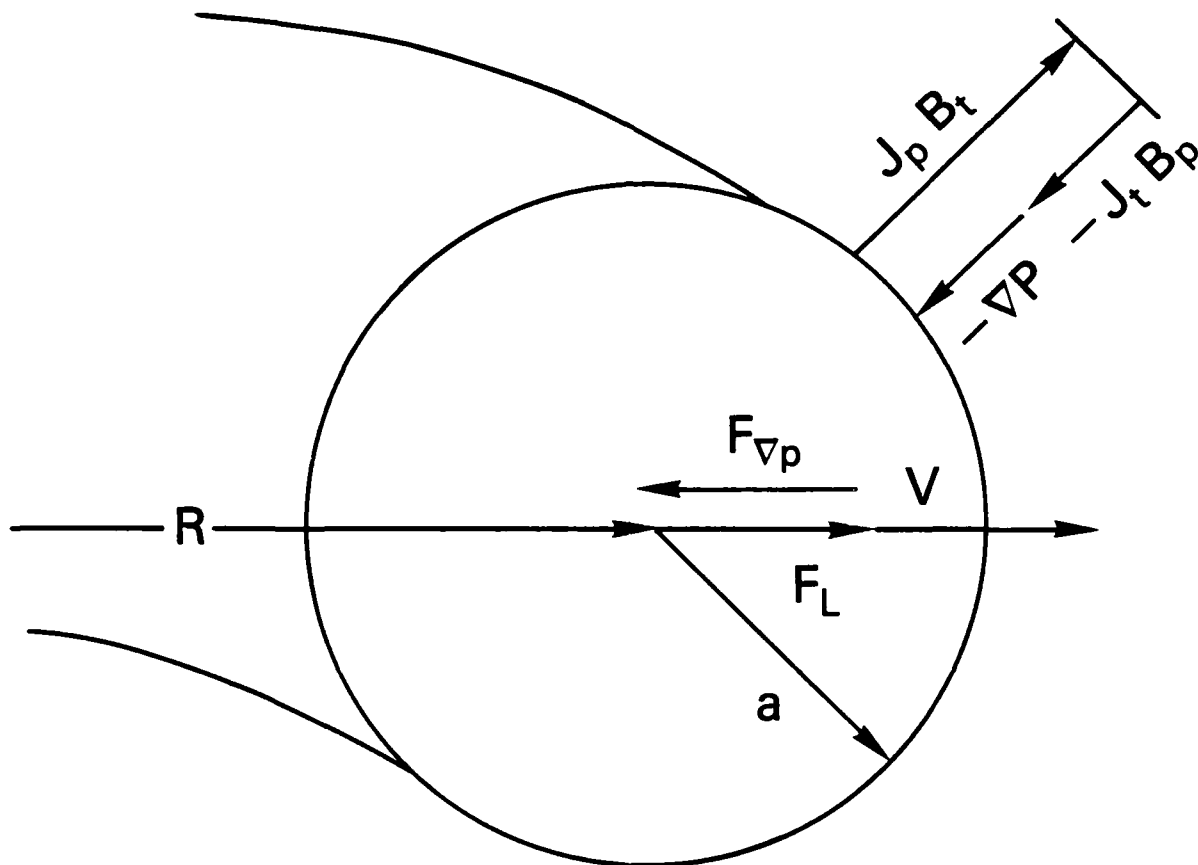   structure need be specified below the photosphere.

Fig. 2   Forces acting on a toroidal current loop. The components
J_pB_t, $\underline{\nabla}p$, and J_tB_p act along the minor radius (a). The "toroidal
forces" acting along the major radius (R) are $F_{\underline{\nabla}p}$, the pressure
force and F_L, the Lorentz force. At high velocities, the drag
force F_d acts in the opposite direction to $\underline{V}$. The drag force due
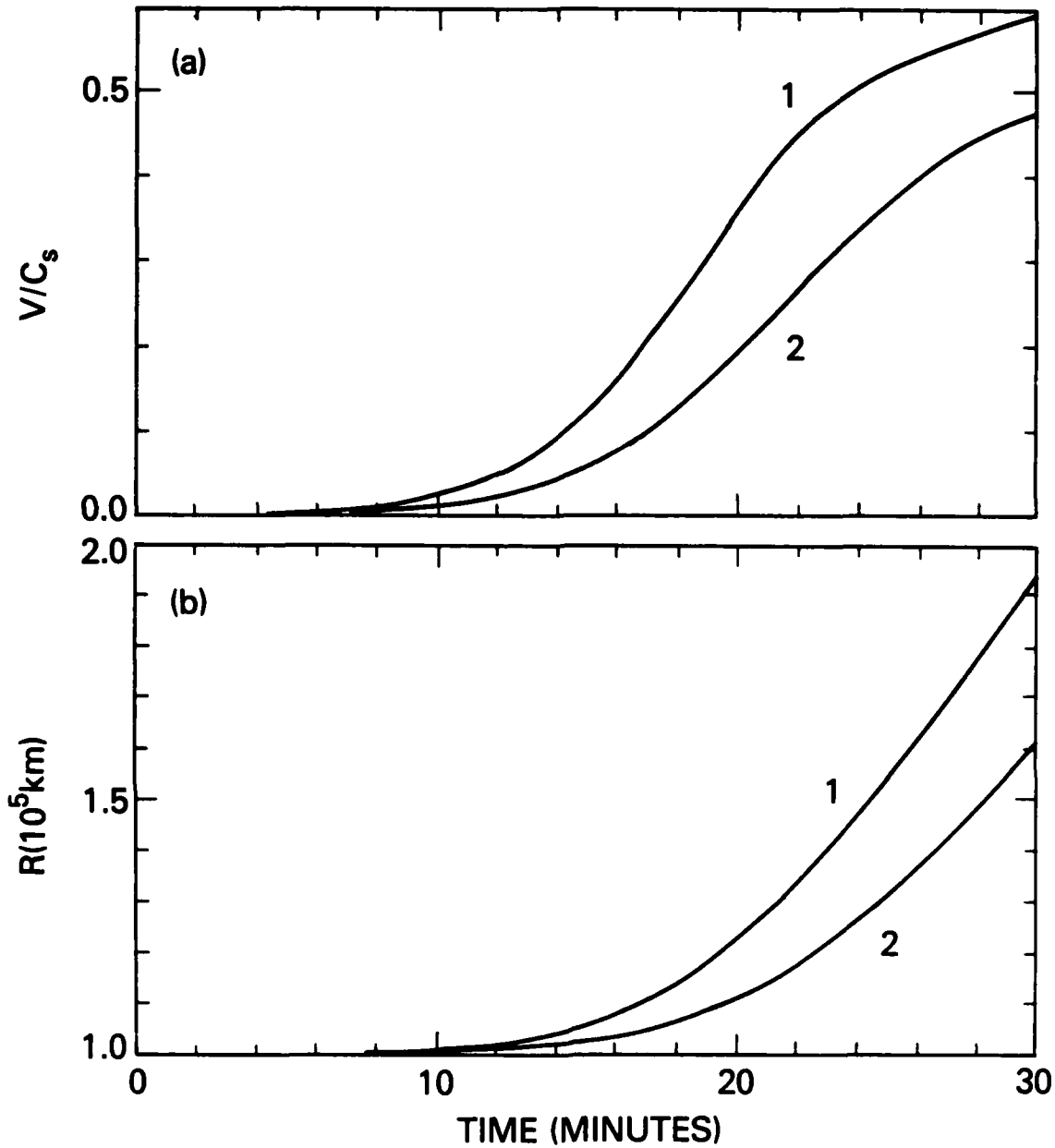to minor radial expansion is neglected.

Fig. 3   Behavior of a model loop initially in equilibrium with $R = 10^5$ km
and $a = 2 \times 10^4$ km. $\epsilon_{cr} = 0.2$ (eq. [22]). For both figures, Curve
1 is $\epsilon = 0.01$ and Curve 2 is $\epsilon = 0.05$.   (a)Velocity profile
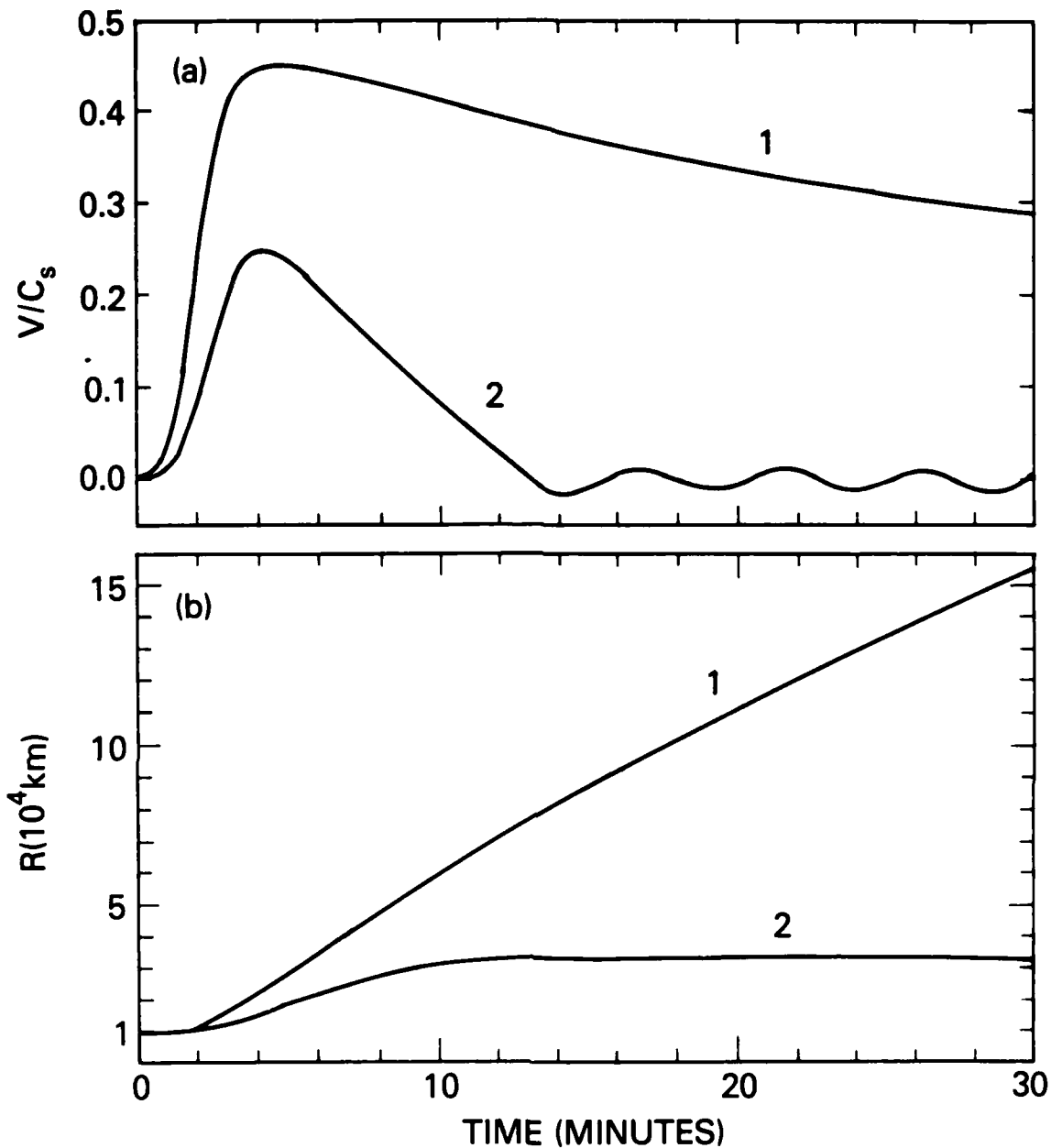normalized to the sound speed $C_s \approx 2.4 \times 10^2$ km sec^{-1}. (b)Major
radius profile.

Fig. 4   Behavior of a model loop initially in equilibrium with $R = 10^4$km
and $a = 2 \times 10^3$km. $\varepsilon_{cr} = 0.1$ (eq. [22]). Curve 1 is $\varepsilon = 0.01$ and
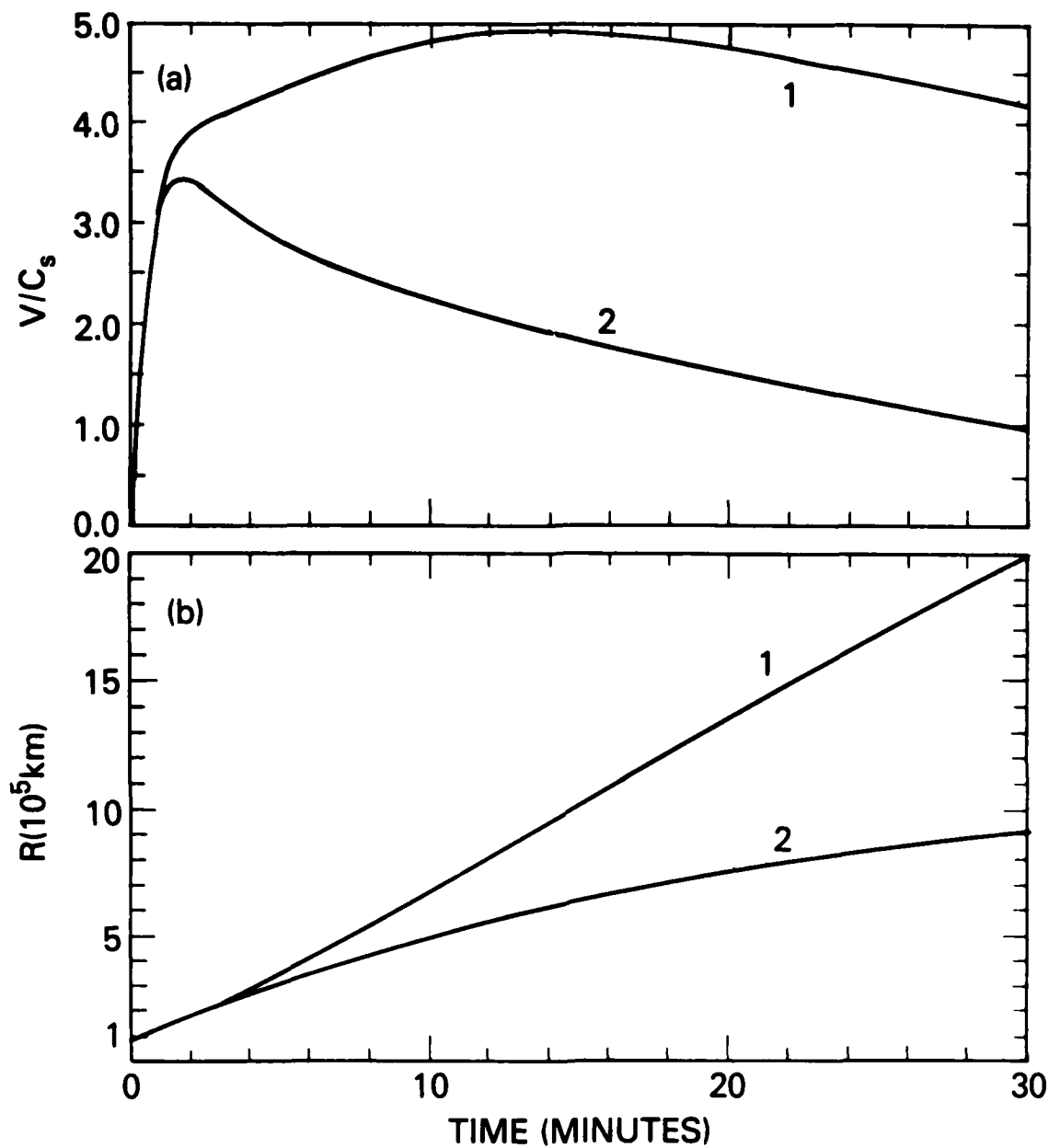Curve 2 is $\varepsilon = 0.05$. (a)Velocity profile. (b)Major radius
profile.

Fig. 5 Behavior of a nonequilibrium model loop with $R = 10^5$km and $a = 2 \times 10^4$km. The quantity ϵ_{cr} does not apply to nonequilibrium loops. Curve 1 is $\epsilon = 0.01$ and Curve 2 is $\epsilon = 0.1$. (a)Velocity profile. (b)Major radius profile.
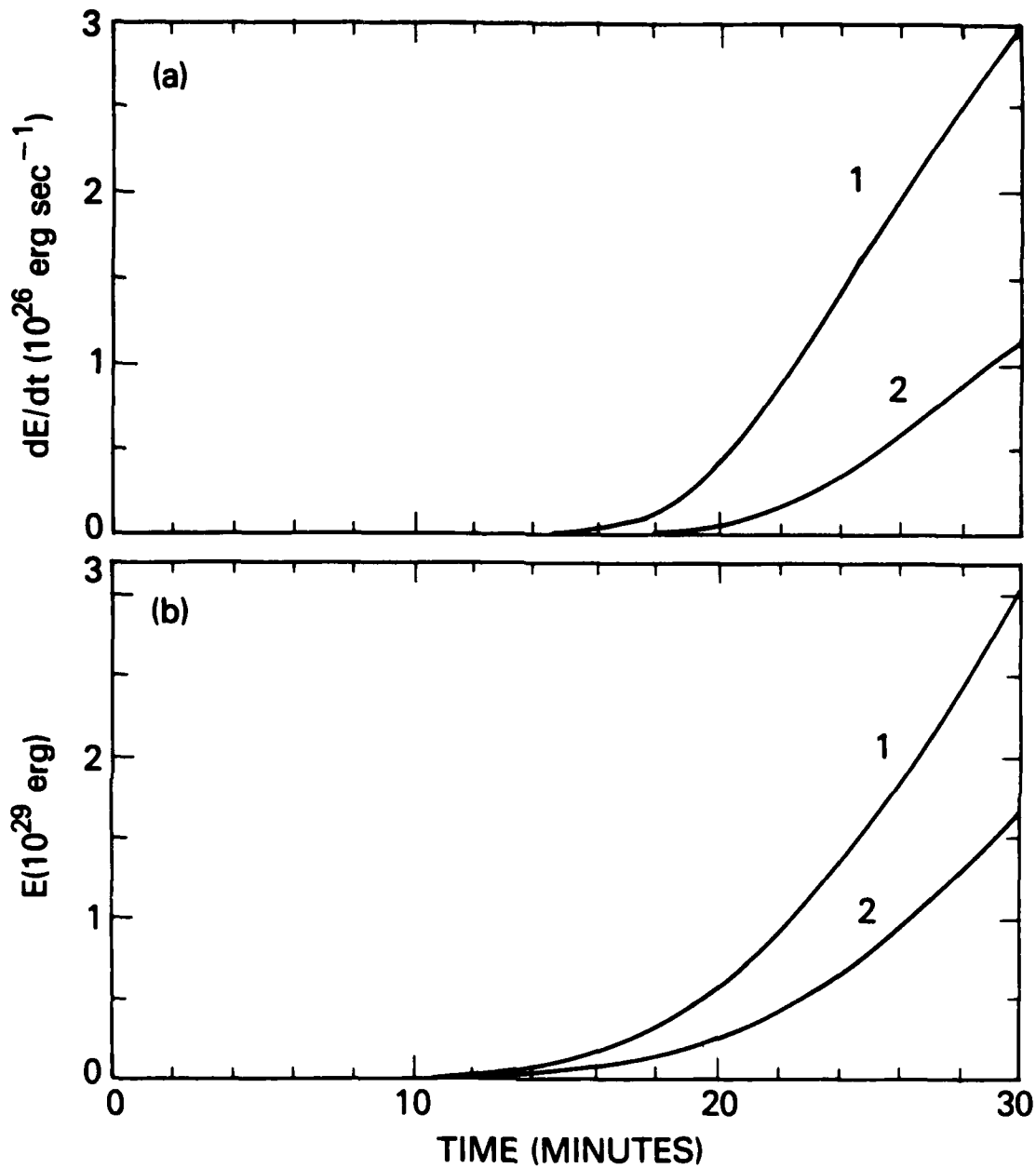
Fig. 6   Magnetic energy released by the model loop of Fig. 3 ($R = 10^5$km and $a = 2 \times 10^4$km). Curve 1 is $\epsilon = 0.01$ and Curve 2 is $\epsilon = 0.05$. (a)Rate of drag heating near the apex. (b)Total magnetic energy released as drag heating and kinetic energy. Drag heating is roughly one-half of the total energy released.

31

Fig. 7   Magnetic energy released by the model loop of Fig. 4 ($R = 10^4$km and $a = 2 \times 10^3$km). Curve 1 is $\varepsilon = 0.01$ and Curve 2 is $\varepsilon = 0.05$. (a)Rate of drag heating near the apex. (b)Total magnetic energy released as drag heating and kinetic energy. Drag heating is roughly one-half of the total energy released.
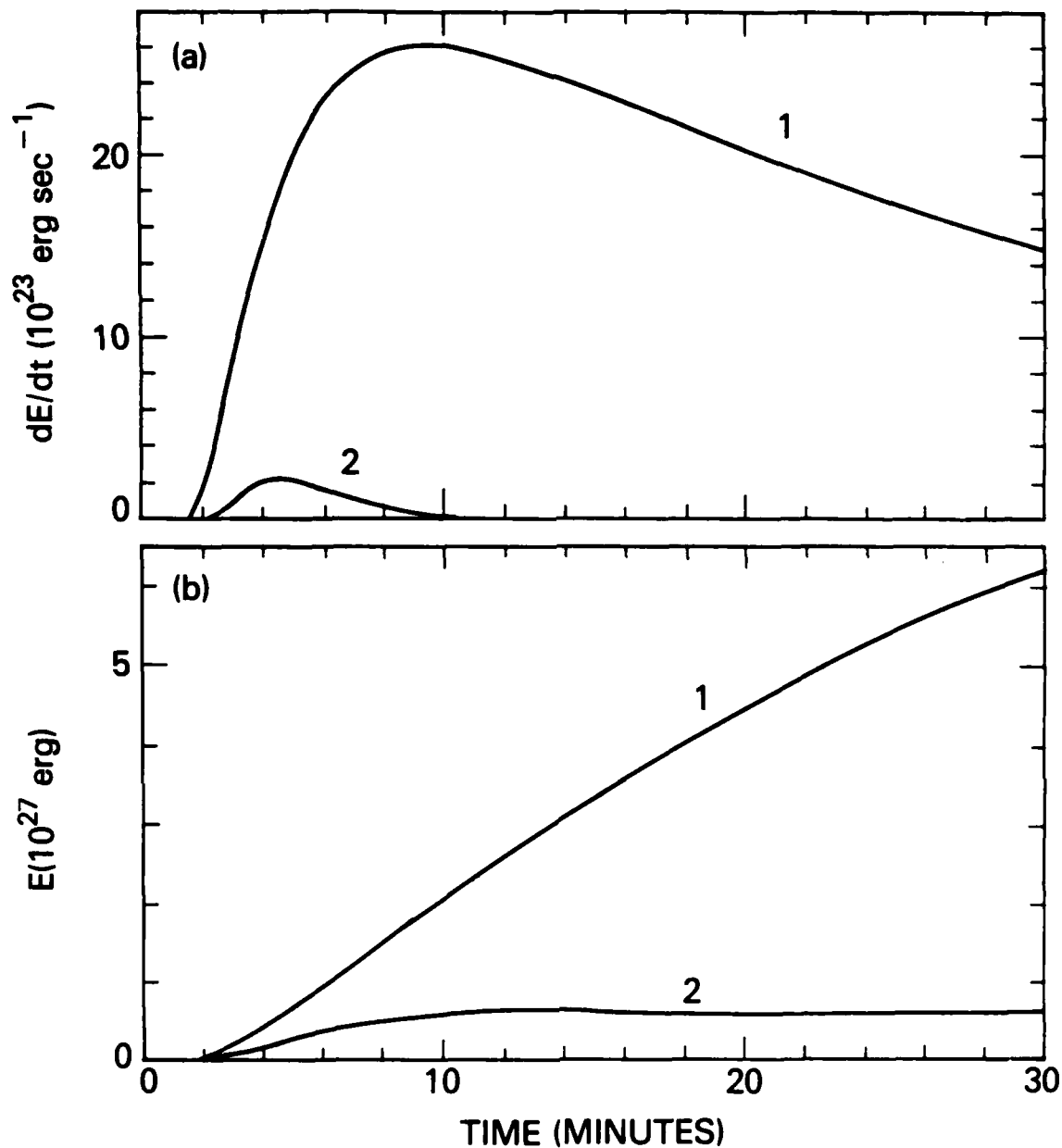
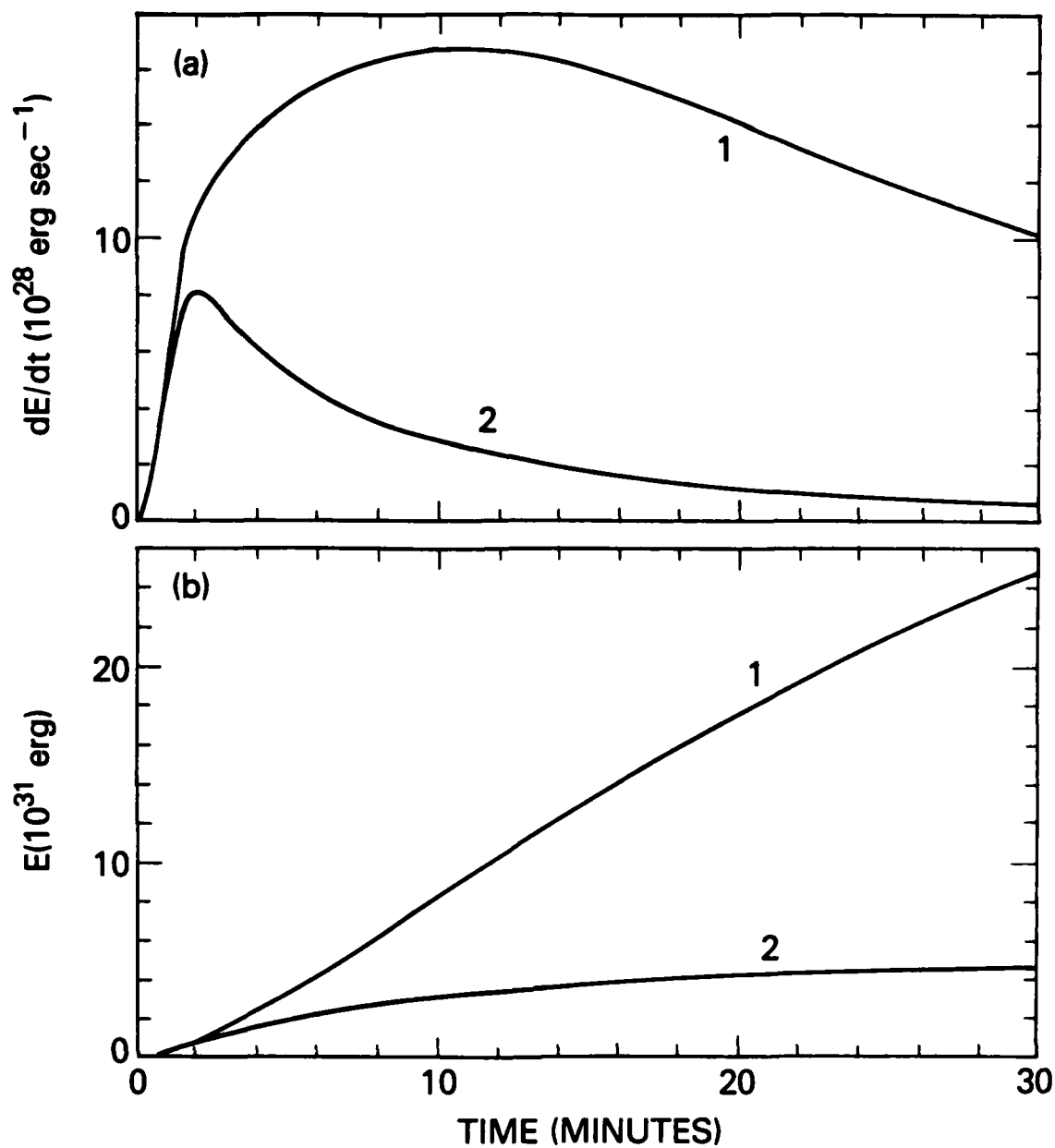Fig. 8   Magnetic energy released by the nonequilibrium loop of Fig. 5 (R = 10^5km and a = 2 x 10^4km). Curve 1 is ε = 0.01 and Curve 2 is ε = 0.1.   (a)Rate of drag heating near the apex. (b)Total magnetic energy released as drag heating and kinetic energy.

DISTRIBUTION LIST
(Unclassified Only)

DISTRIBUTE ONE COPY EACH TO THE FOLLOWING PEOPLE (UNLESS OTHERWISE NOTED)

DIRECTOR
NAVAL RESEARCH LABORATORY
WASHINGTON, DC 20375-5000
    CODE 4700 (26 CYS)
    CODE 4701
    CODE 4780 (50 CYS)
    CODE 4750 (P. RODRIGUEZ)
    CODE 4100
    CODE 4172
    CODE 4173
    CODE 4160
    CODE 4175A
    CODE 4175C
    CODE 4175M
    CODE 4170

OFFICE OF NAVAL RESEARCH
WASHINGTON, DC 22203
    C. ROBERSON

COMMANDING OFFICER
OFFICE OF NAVAL RESEARCH
WESTERN REGIONAL OFFICE
1030 EAST GREEN STREET
PASADENA, CA 91106
    R. BRANDT

NASA HEADQUARTERS
CODE EE
WASHINGTON, DC 20546
    S. SHAWHAN
    D. BUTLER
    T. EASTMAN

NASA/GODDARD SPACE FLIGHT CENTER
GREENBELT, MD 20771
    M. GOLDSTEIN, CODE 692
    T. NORTHROP, CODE 665
    T. BIRMINGHAM, CODE 695.1
    A. FIGUERO VINAS, CODE 692
    SHING F. FUNG, CODE 696
    D.S. SPICER, CODE 682
    J. DAVILA, CODE 682

AEROSPACE CORPORATION
A6/2451, P.O. BOX 92957
LOS ANGELES, CA 90009
    A. NEWMAN
    D. GORNEY
    M. SCHULZ
    J. FENNEL

BELL LABORATORIES
MURRAY HILL, NJ 07974
    A. HASEGAWA
    L. LANZEROTTI

LAWRENCE LIVERMORE LABORATORY
UNIVERSITY OF CALIFORNIA
LIVERMORE, CA 94551
    LIBRARY
    J. DEGROOT
    B. LANGDON
    R. BRIGGS
    D. PEARLSTEIN

LOS ALAMOS NATIONAL LABORATORY
P.O. BOX 1663
LOS ALAMOS, NM 87545
    S.P. GARY
    K. QUEST
    J. BRACKBILL
    J. BIRN
    D. FORSLUND
    J. KINDEL
    D. WINSKE
    J.T. GOSLING

LOCKHEED RESEARCH LABORATORY
3251 HANOVER STREET
PALO ALTO, CA 94304
    M. WALT
    L.W. ACTON

NATIONAL SCIENCE FOUNDATION
ATMOSPHERIC RESEARCH SECTION
WASHINGTON, DC 20550
    D. PEACOCK

UNIVERSITY OF ALASKA
GEOPHYSICAL INSTITUTE
FAIRBANKS, AK 99701
    LIBRARY
    S. AKASOFU
    J. KAN
    L. LEE

UNIVERSITY OF ARIZONA
DEPT. OF PLANETARY SCIENCES
TUCSON, AZ 85721
    J.R. JOKIPII

UNIVERSITY OF CALIFORNIA, S.D.
LAJOLLA, CA 92037
  (PHYSICS DEPARTMENT):
    T. O'NEIL
    J. WINFREY
    H.S. HUDSON, MC C-011
    LIBRARY

UNIVERSITY OF CALIFORNIA
SPACE SCIENCE LABORATORY
BERKELEY, CA 94720
    M. TEMERIN
    F. MOZER

UNIVERSITY OF CALIFORNIA
PHYSICS DEPARTMENT
IRVINE, CA 92664
    LIBRARY
    G. BENFORD
    N. ROSTOKER
    C. ROBERTSON

UNIVERSITY OF CALIFORNIA
LOS ANGELES, CA 90024
  (PHYSICS DEPARTMENT):
    J.M. DAWSON
    J.G. MORALLES
    W. GEKELMAN
    R. STENZEL
    F. CHEN
    M. ASHOUR-ABDALLA
    LIBRARY
    R. WALKER
  (INSTITUTE OF GEOHPYSICS
AND PLANETARY PHYSICS):
    LIBRARY
    C. KENNEL
    F. CORONITI

UNIVERSITY OF CHICAGO
ENRICO FERMI INSTITUTE
CHICAGO, IL 60637
    E.N. PARKER
    I. LERCHE
    LIBRARY

UNIVERSITY OF COLORADO
DEPT. OF ASTRO-GEOPHYSICS
BOULDER, CO 80309
    M. GOLDMAN
    E. ZWEIBEL
    LIBRARY

CORNELL UNIVERSITY
SCHOOL OF APPLIED AND
ENGINEERING PHYSICS
COLLEGE OF ENGINEERING
ITHACA, NY 14853
    LIBRARY
    R. SUDAN
    B. KUSSE
    H. FLEISCHMANN
    R. LOVELACE

HARVARD UNIVERSITY
CENTER FOR ASTROPHYSICS
60 GARDEN STREET
CAMBRIDGE, MA 02138
    G.B. FIELD
    R. ROSNER
    K. TSINGANOS
    G.S. VAIANA

UNIVERSITY OF IOWA
IOWA CITY, IA 52240
    C.K. GOERTZ
    L.A. FRANK
    K. NISHIKAWA
    N. D'ANGELO
    C. HUANG

UNIVERSITY OF MARYLAND
PHYSICS DEPARTMENT
COLLEGE PARK, MD 20742
    K. PAPADOPOULOS
    H. ROWLAND
    C. WU

UNIVERSITY OF MINNESOTA
SCHOOL OF PHYSICS
MINNEAPOLIS, MN 55455
    LIBRARY
    J.R. WINCKLER
    P. KELLOGG
    R. LYSAK

UNIVERSITY OF CALIFORNIA
DEPT. OF PHYSICS
IRVINE, CA 92717
    G. VAN HOVEN
    L. SPARKS

M.I.T.
CAMBRIDGE, MA 02139
    LIBRARY
  (PHYSICS DEPARTMENT):
    B. COPPI
    V. GEORGE
    G. BEKEFI
    T. CHANG
    T. DUPREE
    R. DAVIDSON
  (ELECTRICAL ENGINEERING
  DEPARTMENT):
    R. PARKER
  (R.L.E):
    LIBRARY
  (SPACE SCIENCE):
    READING ROOM

UNIVERSITY OF NEW HAMPSHIRE
DEPARTMENT OF PHYSICS
DURHAM, NH 03824
  R.L. KAUFMAN
  J. HOLLWEG

PRINCETON UNIVERSITY
PRINCETON, NJ 08540
  PHYSICS LIBRARY
  PLASMA PHYSICS LAB. LIBRARY
  F. PERKINS
  T.K. CHU
  H. OKUDA
  R. WHITE
  R. KULSRUD
  H. FURTH
  S. YOSHIKAWA
  P. RUTHERFORD

RICE UNIVERSITY
HOUSTON, TX 77001
  SPACE SCIENCE LIBRARY
  T. HILL
  R. WOLF
  P. REIFF

STANFORD UNIVERSITY
CENTER FOR SPACE SCIENCE
AND ASTROPHYSICS
STANFORD, CA 94305
  P.A. STURROCK
  J. KLIMCHUK

STEVENS INSTITUTE OF TECHNOLOGY
HOBOKEN, NJ 07030
  B. ROSEN
  G. SCHMIDT
  M. SEIDL

UNIVERSITY OF TEXAS
AUSTIN, TX 78712
  W. DRUMMOND
  W. HORTON

THAYER SCHOOL OF ENGINEERING
DARTMOUTH COLLEGE
HANOVER, NH 03755
  BENGT U.O. SONNERUP
  M. HUDSON

UTAH STATE UNIVERSITY
DEPT. OF PHYSICS
LOGAN, UT 84322
  ROBERT W. SCHUNK

UNIVERSITY OF THESSALONIKI
DEPARTMENT OF PHYSICS
GR-54006 THESSALONIKI,
GREECE
  L. VLAHOS

NASA MARSHALL SPACE
FLIGHT CENTER
HUNTSVILLE, AL 35812
  C.H. ANN, ES-52
  J. PORTER, ES-52
  J. FONTENLA, ES-52

UNIVERSITY OF ALABAMA, HUNTSVILLE
DEPARTMENT OF PHYSICS
HUNTSVILLE, AL 35899
  A.G. EMSLIE

MIDDLEBURY COLLEGE
DEPT. OF PHYSICS
MIDDLEBURY, VT 05733
  R. WOLFSON

UNIVERSITY OF HAWAII
INSTITUTE FOR ASTRONOMY
2680 WOODLAWN DRIVE
HONOLULU, HI 96822
  G. FISHER
  D. CHOU
  R. CANFIELD

HIGH ALTITUDE OBSERVATORY/NCAR
P.O. BOX 3000
BOULDER, CO 80307
  A. CHOUDHURI
  E. HILDNER
  B.C. LOW
  A. HUNDHAUSEN
  T.E. HOLZER
  R.M. MACQUEEN

INSTITUTE OF THEORETICAL PHYSICS
RUHR-UNIVERSITAT BOCHUM
4630 BOCHUM, WEST GERMANY
    K. SCHINDLER

THE UNIVERSITY OF ST. ANDREWS
APPLIED MATHEMATICS DEPT.
ST. ANDREWS, SCOTLAND
    E.R. PRIEST

UNIVERSITY OF TEXAS, AUSTIN
DEPT. OF PHYSICS
AUSTIN, TX 78712
    T. TAJIMA
    R.S. STEINOLFSON

BERKELEY RESEARCH ASSOCIATES
290 GREEN ROCK DRIVE
BOULDER, CO 80302

APPLIED PHYSICS LABORATORY
THE JOHNS HOPKINS UNIVERSITY
LAUREL, MD 20707
    A.T.Y. LUI
    D.G. MITCHELL
    D.A. BATCHELOR

SCIENCE   APPLICATIONS   INTERNATIONAL
CORPORATION
10260 CAMPUS POINT DRIVE
SAN DIEGO, CA 92121
    D.C. BARNES
    D.D. SCHNACK
    Z. MIKIC

END

3-88

DTIC